Journal of Power Sources 195 (2010) 7808–7817

Contents lists available at ScienceDirect

Journal of Power Sources

journal homepage: www.elsevier.com/locate/jpowsour

Novel functionalized carbon nanotubes as cross-links reinforced vinyl ester/nanocomposite bipolar plates for polymer electrolyte membrane fuel cells

Shu-Hang Liao[a], Min-Chien Hsiao[a], Chuan-Yu Yen[a], Chen-Chi M. Ma[a,*], Shuo-Jen Lee[b], Ay Su[b], Ming-Chi Tsai[c], Ming-Yu Yen[a], Po-Lan Liu[a]

[a] Department of Chemical Engineering, National Tsing Hua University, Hsin-Chu 30013, Taiwan, ROC
[b] Fuel Cell Center, Yuan Ze University, Tao-Yuan 32003, Taiwan, ROC
[c] Department of Engineering and System Science, National Tsing Hua University, Hsin-Chu 30013, Taiwan, ROC

ARTICLE INFO

Article history:
Received 12 August 2009
Received in revised form 7 October 2009
Accepted 11 October 2009
Available online 30 October 2009

Keywords:
Functionalized carbon nanotubes
Vinyl ester
Cross-link
Nanocomposite
Bipolar plate
Fuel cells

ABSTRACT

In this study, the novel functionalized multi-walled carbon nanotubes (MWCNTs) are used as cross-links between MWCNTs–vinyl ester interfaces to achieve homogeneous dispersion and strong interfacial bonding for developing fully integrated MWCNTs–vinyl ester nanocomposite bipolar plates. POAMA (i.e. poly(oxyalkylene)-amines (POA) bearing maleic anhydride (MA)) are grafted onto the MWCNTs by amidization reaction, forming MWCNTs-POAMA. In the MWCNTs-POAMA/vinyl ester nanocomposites, MWCNT-POAMAs react with vinyl ester and become part of the cross-linked structure, rather than just a separate component. It is found that the MWCNTs-POAMA exhibited better dispersion in the vinyl ester matrix than those of pristine MWCNTs. Moreover, the results demonstrate that the mechanical and electrical properties of the vinyl ester nanocomposite bipolar plate are improved dramatically. The ultimate flexural strength, unnotched impact strength, in-plane electrical conductivity and contact resistance of the MWCNTs-POAMA/vinyl ester nanocomposite bipolar plate are increased by 45%, 90%, 315% and 28%, respectively. In addition, the maximum current and power densities of the single fuel cell test using the MWCNTs-POAMA/vinyl ester nanocomposite bipolar plates is enhanced from 1.03 to 1.23 A cm^{-2} and from 0.366 to 0.518 W cm^{-2}, respectively, which suggested that a higher electron transfer ability for polymer electrolyte membrane fuel cell applications can be achieved.

1. Introduction

The polymer electrolyte membrane fuel cells (PEMFCs) exhibit the most promising alternative source of energy for a variety of portable electronic devices, stationary and vehicle applications [1–3]. To generate useful currents and voltages, individual single fuel cells are connected in series to form stacks of cells. Thus, as one of the key components of PEMFCs, bipolar plates must exhibit excellent electrical conductivity as a current collector and adequate mechanical strength to resist the clamping force while the stack was assembled. Traditionally, the most used material for bipolar plate is prepared by machining graphite plate because it provides excellent corrosion resistance, low bulk density and high electrical conductivity [4–6]. However, the brittleness and difficulties in machining graphite plates often limit the use of thin bipolar plates for reducing the stack weight [6,7]. Additionally, the main difficulty in using graphite to produce bipolar plate is the time consuming and costly step of machining flow channels in the surfaces [8].

Because of the costly machining step associated with graphite plates, numerous alternative materials have been developed and investigated to reduce the cost as well as the weight of the fuel cell. Metallic materials such as stainless steel, aluminum, titanium and alloy or a protective coating layer on the surfaces of the plates have been widely investigated [9–11]. Metallic plates typically have high bulk electrical conductivity, good thermal conductivity, and excellent mechanical properties [7,12]. However, a number of disadvantages are associated with metallic materials, including high density, high cost of machining, poor corrosion resistance and the possibility for metal ions to leach into the membrane-electrode assembly (MEA) [7,8]. Therefore, attributes of a suitable material for bipolar plates in PEMFC include:

(1) High electrical conductivity (>100 S cm^{-1}) [13].
(2) Good flexural strength (>25 MPa) [13].
(3) High impact strength (>40.5 J m^{-1}) [14].
(4) Good chemical stability and corrosion resistance under PEMFC operating conditions (<1 μA cm^{-2}) [15].

* Corresponding author. Tel.: +886 3571 3058; fax: +886 3571 5408.
E-mail addresses: ccma@che.nthu.edu.tw, d9532814@oz.nthu.edu.tw (C.-C.M. Ma).

0378-7753/$ – see front matter.
doi:10.1016/j.jpowsour.2009.10.020

(5) High thermal conductivity to achieve stack cooling (>10 W (mK)$^{-1}$) [14].
(6) Low weight, especially for transportation application.
(7) Low cost.

In place of graphite bipolar plates, graphite-based polymer composite bipolar plates are made from a combination of graphite, carbon powder filler or various fibers and a polymer resin. Comparing to graphite bipolar plates, graphite-based polymer composite bipolar plates offer advantages of lower cost, higher flexibility, greater processability, and gas flow channels can be molded directly into the plate, eliminating the need for machining [16,17]. However, high loading of carbon or graphite fillers must be incorporated into the composite bipolar plate to meet the minimum electrical conductivity required. Unfortunately, high carbon loading causes a substantial reduction in strength and ductility of composite bipolar plate, resulting in the difficulty of making thin plates required for high stack power densities [2,18,19]. Therefore, several reinforced composite bipolar plates have been developed, including carbon–carbon composites [20], conventional conducting fillers/polymer matrix [7,21–23], thermosetting or thermoplastic polymer blending with multi-walled carbon nanotubes (MWCNTs) for use in composite materials [1,3,18,24–27]. Nevertheless, polymer composites incorporated with CNTs possess excellent electrical conductivity and mechanical properties which may be the suitable materials for composite bipolar plates.

Because of their intrinsic high-aspect ratio, high mechanical strength, and excellent electrical and thermal conductivity, CNTs have been attracted for high-performance and multifunctional polymer composite applications [28–33]. However, several studies [34–40] have shown that only weak interfacial bonding existed between pristine CNTs and matrix, which is resulted from the atomically smooth non-reactive surface characteristics of CNTs, and thus, limiting the load-transfer ability from the matrix to CNTs. Due to the lack of interfacial bonding between polymers and MWCNTs, the MWCNTs were commonly aggregated into bundles and ropes, restricting their utilization in polymer composites [34]. Therefore, the interfacial interaction between CNTs and polymer, and the ability to disperse the CNTs homogeneously in the matrix will be the challenges in order to take the full advantage of the extraordinary properties of CNTs [27,28,33–35]. To overcome these difficulties, many researches have investigated the modification of CNTs, including the use of physical blending (by high shear mixing or ultrasonication) with the aid of surfactants [28], chemical covalent modification [24–35], or wrapping polymer on the CNT wall [36]. Among these modification techniques of CNTs, the chemical functionalization of CNTs is being investigated actively [37]. Nevertheless, the most effective method utilizing this approach is based on the incorporation of the CNTs into matrices via chemical bonding so that surface-functionalized CNTs may serve as cross-links which will be integrated into thermoset resin network, rather than just as separated fillers [27,28,33,35]. Zhu et al. [33] grafted curing agent on the SWCNT surface to reinforce epoxy, and obtained a 25% enhancement in tensile strength and more than 30% increase in Young's modulus with only 1 wt% loading of functionalized CNTs. Tseng et al. [27] functionalized MWCNTs by grafting maleic anhydride onto the MWCNT walls and subsequently reacted with diamine, which acted as a curing agent for MWCNTs/epoxy composites. With only 1 wt% of functionalized CNTs in the epoxy/MWCNTs composites, the average tensile strength was 50% higher than neat epoxy and more than 42% improvement in tensile modulus and two orders of magnitude higher than the pristine MWCNTs/epoxy composites, respectively. Sun et al. [28] found that SWCNT surface grafted with polyamidoamine generation-o (PMMA-o) dendrimers causing chemically bridge between SWCNTs and epoxy, consequently, the dispersion and adhesion of SWCNTs in epoxy were improve effectively. Furthermore, the results exhibit that the incorporation of functionalized SWCNTs leads to increase the Young's modulus and tensile strength by 27% and 17%, respectively. However, so far, the idea associated with functionalized CNTs as a curing agent for the thermoset vinyl ester resin has not been reported yet.

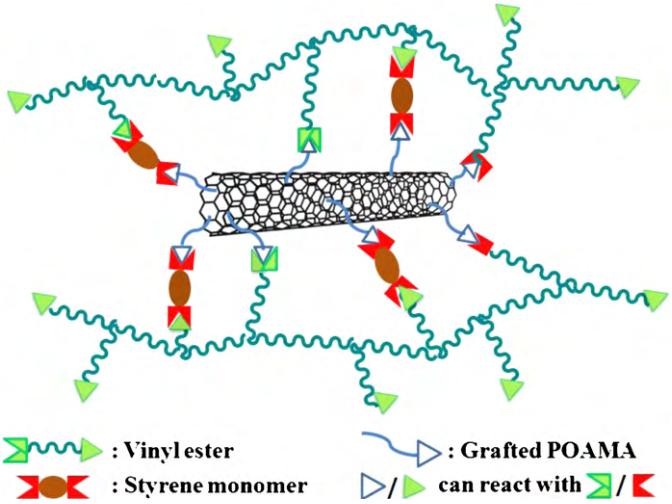

Fig. 1. The cross-linking structure of functionalized carbon nanotubes reacted with vinyl ester and styrene monomer.

Herein, this study proposed the idea of the functionalization of MWCNTs and further to develop a novel MWCNTs/vinyl ester polymer composites system with direct cross-linking between the matrix and the functionalized MWCNTs. The functionalized MWCNTs were prepared by grafting poly(oxyalkylene amine) (POA) bearing maleic anhydride (MA) (POAMA) synthesized in our previous study [17]. The terminal unsaturated double bonds of the POAMA attached to the MWCNTs can readily react with the vinyl ester and act as cross-links for vinyl ester matrix, while bifunctional vinyl ester continues to react with the styrene monomer curing agents added, as illustrated in Fig. 1 schematically. In this nanocomposite, the grafted polymer chains penetrate with vinyl esters and become a part of vinyl ester matrix and bridging the connection of MWCNTs to the matrix. In this method, vinyl esters stick strongly to the MWCNTs and increase the vinyl ester-MWCNT interfacial interaction [27,28,33]. Due to the multiple unsaturated double bonds of POAMA attached to the MWCNTs, the resulting vinyl ester nanocomposite bipolar plates will form a high cross-linked structure with covalent bonds between the MWCNTs and vinyl ester [33]. Furthermore, the effects of MWCNT dispersion on the mechanical and electrical properties of MWCNTs/vinyl ester nanocomposite bipolar plates were reported in this paper. The single fuel cell performance test of these MWCNTs/vinyl ester nanocomposite bipolar plates was also evaluated.

2. Experimental

2.1. Materials

The MWCNTs (trade name: $C_{tube}100$) with a purity of 95% and 150–250 m^2 g^{-1} of surface area were obtained from the CNT Co., Ltd., Korea. The diameters of MWCNTs are 10–50 nm and the lengths are 1–25 μm. Poly(oxyalkylene)-diamines (POA) were purchased from Huntsman Chemical Co., Philadelphia, Pennsylvania, U.S.A., include poly(oxypropylene) (POP)-backboned diamines with a molecular weight of 2000 g mol^{-1}. Maleic anhydride (MA) was obtained from Showa Chemical Co., Gyoda City, Saotama, Japan. Phenolic-novolac epoxy-based vinyl ester (VE) was pro-

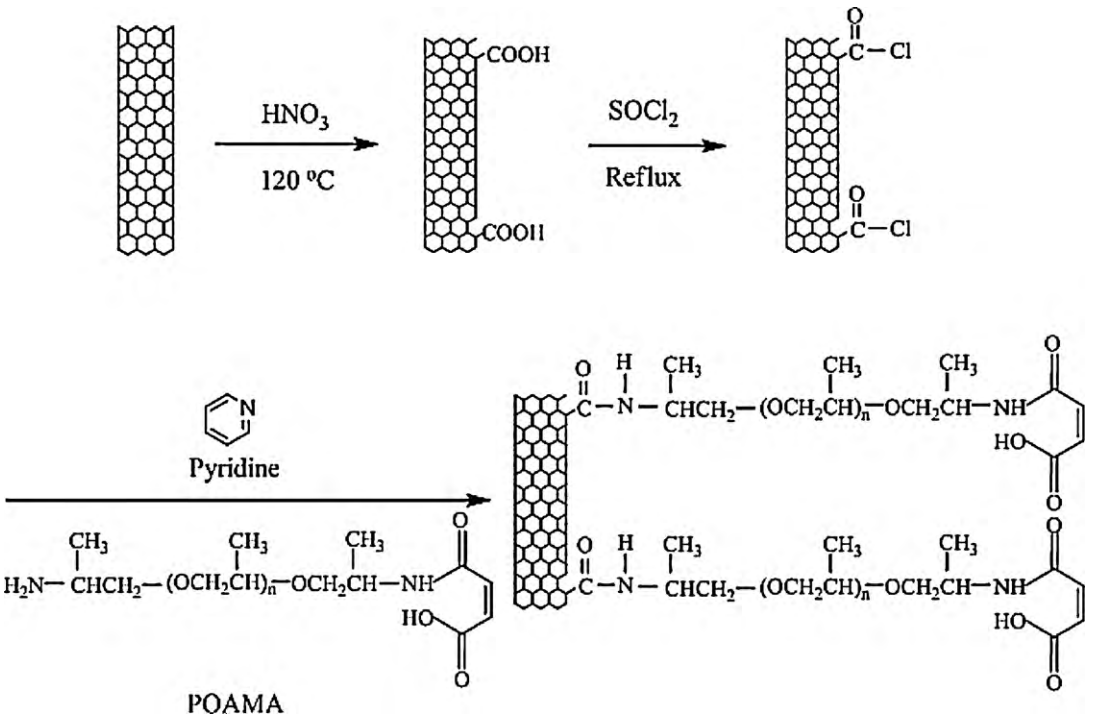

Scheme 1. Overall synthesis for MWCNTs-POAMA.

vided by Swancor Co., Taiwan. Graphite powder was obtained from Great Carbon Co., Ltd., Taiwan. The density of the graphite power is 1.88 g cm^{-3} and the particle size is less than 1000 μm.

2.2. Preparation of functionalized MWCNTs

Scheme 1 depicts the covalent grafting procedure. Details of the preparation of the POA bearing one MA (abbreviated POAMA) followed the procedure illustrated in our previous study [17]. The oxidized MWCNTs (MWCNTs-COOH) were first achieved according to a HNO_3 washing procedure; 8 g of pristine MWCNTs were boiled in 400 ml of concentrated HNO_3 for 40 min. Then, MWCNTs-COOH were filtered, washed with 600 ml distilled water for several times to remove acid, and dried at 105 °C in an oven. During the second step, MWCNTs-COOH was converted to acid chloride-functionalized MWCNTs by refluxing in thionyl chloride for 72 h, followed by the subsequent reaction with the excess POAMA dissolved in pyridine at 70 °C for 12 h. After the grafting polymerization, the mixture was separated by filtration through 0.2 μm polytetrafluoroethylene (PTFE) membrane and thoroughly washed with anhydrous THF several times to remove the residual POAMA, and then dried in a vacuum oven at 80 °C overnight to remove the solvent. The resulting reaction product was the unsaturated double bonds-terminated derivative of the MWCNTs, denoted as MWCNTs-POAMA.

2.3. Preparation of MWCNTs/VE nanocomposites

To prepare the MWCNTs/VE composites, 6.75 g of VE and 0.162 g of initiator (t-butyl perbenzoate/TPPB) were dissolved in 2.25 g of styrene monomer and 0.1 g of pristine MWCNT and corresponding MWCNTs-COOH and MWCNTs-POAMA was added, respectively.

Table 1
Formulation of BMC material.

Components	Composition	
	Resin composition	BMC composition
Vinyl ester[a] (wt%)	75	30
Low profile agent (wt%)	8	
Styrene monomer (wt%)	17	
TBPB (phr)[b]	1.8	
Zinc stearate (phr)	3.5	
Magnesium oxide (phr)	1.8	
MWCNTs (wt%)	0–2	
Graphite powder (wt%)		70
Total (wt%)		100

[a] Chemical structure of phenolic-novolac epoxy-based vinyl ester is as follows:

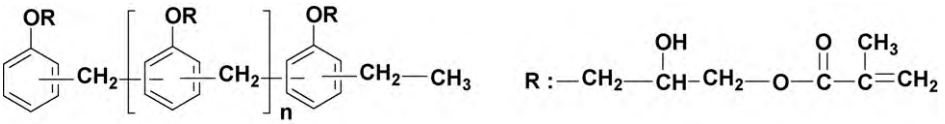

[b] phr: parts per hundred parts of resin, based on amount of vinyl ester, low profile agent and styrene monomer.

The mixture was dispersed in the solution via sonication for 10 min. Then, the prepared MWCNTs/VE mixture containing pristine MWCNTs, MWCNTs-COOH and MWCNTs-POAMA, respectively, was poured into an aluminum plate, and cured by increasing the temperature slowly from 80 to 120 °C in an oven. Finally, three MWCNTs/VE nanocomposites were completely cured by evacuation at 140 °C for 24 h.

2.4. Preparation of MWCNTs/VE nanocomposite bipolar plates

The bulk molding compound (BMC) was prepared by mixing various MWCNTs/VE mixtures, low profile agent (PS/SM series), styrene monomer, thickening agent (MgO), release agent (ZnSt) and graphite in a kneader for 30 min. The BMC formulation is summarized in Table 1. The BMC was thickened for 36 h before the hot-pressing process. The processing condition was 140 °C was 5 min. Finally, MWCNTs/VE nanocomposite bipolar plates were successfully fabricated. The dimensions of composite bipolar plate are 30 mm × 30 mm, 3 mm thick. The dimensions of depth and width of the channel are 1 mm × 1 mm.

2.5. Characterization and instruments

Thermogravimetric analysis (TGA) was conducted utilizing a DuPont-TGA951 with a heating rate of 10 °C min^{-1} under N_2 atmosphere. X-ray photoelectron spectra (XPS) measurements were performed using a VG Scientific ESCALAB 220 iXL spectrometer equipped with a hemispherical electron analyzer and an MgKα ($h\nu$ = 1487.7 eV) X-ray source. A small spot lens system allowed the analysis of a sample that was less than 1 mm^2 in area. The dispersion of MWCNTs in vinyl ester was investigated by a field emission-scanning electron microscope (FE-SEM, JEOL JSM-6330, Japan) with an accelerating potential of 15.0 kV. Transmission electron microscope (TEM) analysis was conducted on a PHILPS M100 electron microscope at 200 kV, and the samples for TEM measurements were prepared by one drop casting on carbon-coated copper grids followed by solvent evaporation in air at room temperature. The flexural strength tests were performed based on the procedure of ASTM D-790 by an Instron Model 4468 universal tester and the specimen dimensions were 60.0 mm × 13.0 mm × 3.0 mm ($L \times W \times T$). The in-plane electrical conductivity of the composite bipolar plate was examined with a four point probe detector (C4S-54/5S, Cascade Microtech, Beaverton, Oregon, USA.). An experimental apparatus was used for contact resistance measurement was established [2]. A composite bipolar plate with 30 mm × 30 mm × 3 mm and channel field size of 20 mm × 20 mm was placed between two carbon papers, each of which was in contact with a gold-plated copper plate on the opposite side. The dimensions of carbon papers are 21 mm × 21 mm on the channel field and are 30 mm × 30 mm on the flat side of the plate. The composite bipolar plate was placed under different applied pressures. When a constant current was passed through the two gold-plated copper plates, the difference of potential between the gold-plated copper plates was measured. Half-cell resistance was calculated based on the Ohm's law. A single PEMFC was developed at our laboratory as reported in our previous paper [3]. The catalyst ink for the electrodes was prepared by mixing the catalyst powder (20 wt% Pt/C, E-TEK), Nafion® solution, and iso-propyl alcohol. Then the prepared catalyst ink was sprayed on the wet-proof carbon paper with a platinum loading of 0.4 mg cm^{-2} for the anode and cathode. The membrane-electrode assembly (MEA) was fabricated by placing the electrodes at both sides of pre-treated Nafion® 115 membrane, followed by hot pressing at 140 °C and 200 kg cm^{-2} for 90 s. The active electrode area was 4 cm^2. A single fuel cell was constructed from the prepared MEA, Teflon® gasket, and the prepared composite bipolar plate on both sides of the MEA. The thickness of the composite bipolar plates was 1.2 mm. The operating temperature and pressure of the single fuel cell were 70 °C and 1 atm, respectively. Hydrogen and oxygen gases were fed to the anode and cathode, respectively, after passing through a bubble humidifier, the flow rate ratio of the fuel and the oxidant was 1/1

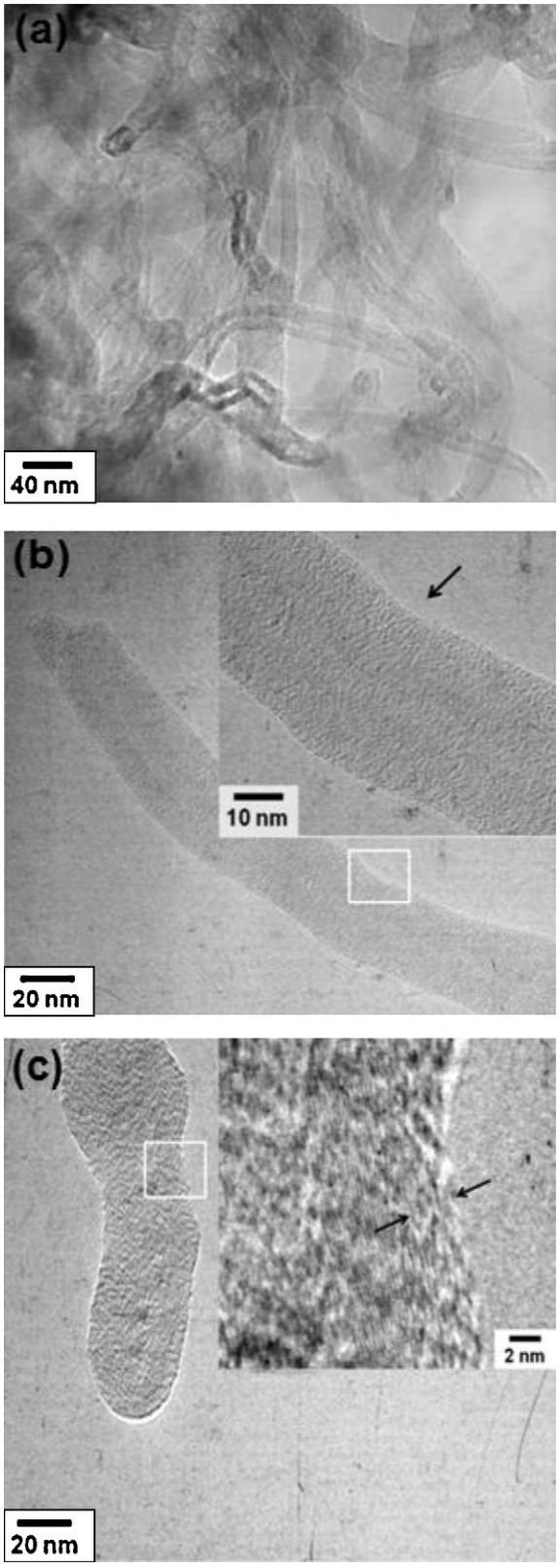

Fig. 2. TEM images of the (a) pristine MWCNTs, (b) MWCNTs-COOH, and (c) MWCNTs-POAMA.

(1 min^{-1}). The performance of the single fuel cell was evaluated by measuring the I–V characteristics using an electronic load (Agilent, N3301A).

3. Results and discussion

3.1. Characteristic of functionalized MWCNTs

Fig. 2 illustrates the TEM images of the morphology and tubular structure of the functionalized MWCNTs, MWCNTs-COOH and MWCNTs-POAMA. Fig. 2(a) shows that the pristine MWCNTs posses a typical tangled structure and crowded bundles. After acid treatment, it can be found that MWCNTs-COOH structural integrity was deteriorated, and the defects of MWCNTs-COOH are observed evidently because of the possible carbon species, including MWCNTs (as can be seen in Fig. 2(b)) [41–44]. In contrast to pristine MWCNTs and MWCNTs-COOH, an organic coating was observed on MWCNTs-POAMA by TEM, as shown in Fig. 2(c). At high magnification, an organic film is visible on the exterior of the MWCNTs. The measured thickness of POAMA coated is varied from 3 to 10 nm. The thickness was observed to vary along the length of the nanotubes. This variation in thickness suggests that the POAMA molecules are not well aligned on the surface of the MWCNTs but entangled, forming multiple layers with varied orientation on the nanotube surface [45].

This work conducts qualitative analysis of XPS to elucidate surface composition of functionalized MWCNTs. The C 1s core level spectra of pristine and functionalized MWCNTs are presented in Fig. 3a. Besides the main sp^2 C═C, the sp^3 C—C peaks of MWCNTs appeared at 284.3–285.1 eV, additional peaks were also shown at higher binding energies for functionalized MWCNTs indicating the presence of carbon atoms bonded to other functional groups. The binding energy peak for the pristine MWCNTs at 286.2 eV is attributed to atmospheric oxidation or residual oxides resulting from the MWCNT purification process [46]. The C 1s spectrum of the MWCNTs-COOH shown in Fig. 3a implies not only the main peaks but also a smaller shoulder peak and a well-separated peak existed at a higher binding energy region. Moreover, the main C 1s peak was based upon integration of the sp^2 C═C peak at 284.3 eV and the sp^3 C—C peak at 285.1 eV, the additional binding energies at 286.1 and 288.7 eV represent the contributions by C—O and O—C═O, respectively [47]. The existence of C 1s peak at 288.7 eV implies the formation of carboxylic groups on the carbon nanotubes. Besides the main C 1s peaks, the resulting C 1s spectrum of MWCNTs-POAMA (Fig. 3a) could be fitted to the additional five different types of carbon functionality [48–49]: carbon bonded to amide/carboxylic acid groups ($\underline{C}H_2C(O)NHR/\underline{C}H_2C(O)OH$ ~285.7 eV), to oxygen ($\underline{C}$—O ~286.5 eV), and to nitrogen (HN—$\underline{C}$H(CH3)—O ~287.3 eV), and carbon in amide groups (RH—N—$\underline{C}$═O ~287.9 eV), respectively. The amidization reaction via carboxylic acid groups is a critical step for the formation of the MWCNTs-POAMA. It is noticeable that the absence of the peak at 288.7 eV is significant since the binding energy of carboxylic groups is expected to decrease significantly when a carboxylic acid is converted to an amide, due to the electron donation from the adjacent nitrogen atom [50]. Thus, the phenomenon we observed in the C 1s spectrum confirmed the formation of an amide linkage on the carbon nanotubes. Furthermore, the peak location and the peak area percentage of the above XPS C 1s results of MWCNTs-POAMA could be examined, as summarized in Table 2. Results are in good agreement with theoretical analysis. Interestingly, since the functionalities of the MWCNTs was anticipated to

Table 2
XPS C 1s curve fitting for MWCNTs-POAMA.

Assignment	MWCNTs-POAMA	
	Peak position (eV)	Peak area percentage (%)
C═C	284.5	48.12
C–C	285.1	21.32
$\underline{C}H_2C(O)NHR/\underline{C}H_2C(O)OH$	285.7	5.22
$\underline{C}$–O	286.5	21.36
HN–$\underline{C}H(CH_3)$–O	287.3	1.99
–N–$\underline{C}$═O	287.9	1.99

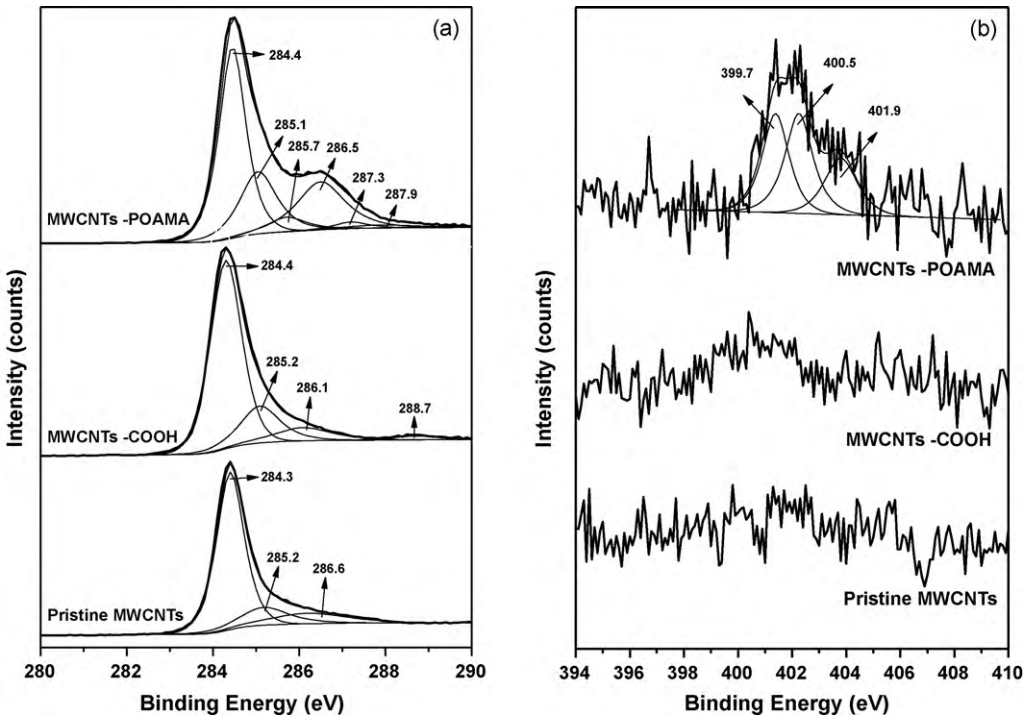

Fig. 3. High-resolution XPS spectra of the surface of pristine MCWNTs, MWNCTs-COOH and MWCNTs-POAMA: (a) C 1s and (b) N 1s.

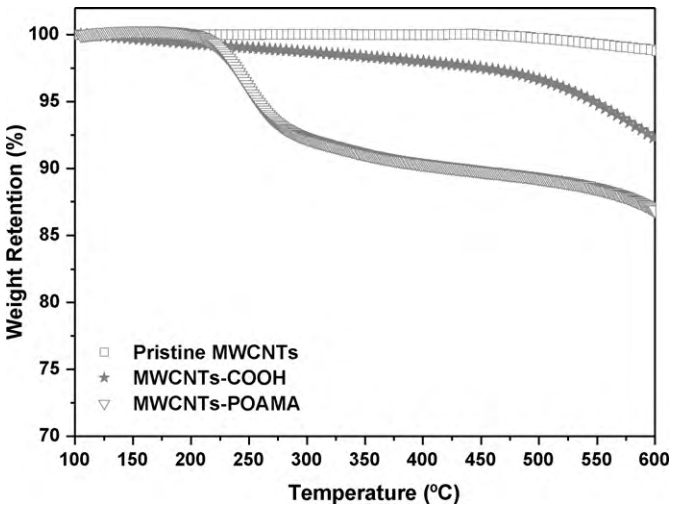

Fig. 4. TGA curves of the pristine and functionalized MWCNTs, MWCNTs-COOH and MWCNTs-POAMA.

obtain HN—CH(CH3)—O and RH—N—C=O structures in equal quantity (Scheme 1), the C 1s spectrum of MWCNTs-POAMA shows that both two structures have a peak area ratio of 1:1. These results indicated that the fitted C 1s peaks are consistent with the POAMA molecule structure linked to the MWCNT surface.

Furthermore, the N 1s core-level XPS spectra confirm the functionalization of MWCNTs-POAMA. The peak-fitting results for three N 1s peaks among the three MWCNT systems are illustrated in Fig. 3b. The N 1s peaks of MWCNTs-POAMA are appeared clearly, which may be attributed to amide groups formed by the amidization reaction, however, which do not occur in the pristine MWCNTs and neither in MWCNTs-COOH. As an example, the low binding energy at 399.7 eV is the characteristic peak of nitrogen of the amide group located at the terminal position of MA-POA chains and the linkage of MA-POA chains and MWCNT walls. The peak at 400.5 eV has a binding energy value 0.8 eV which is higher than 399.7 eV, that is attributed to the additional hydrogen-bonding interaction involving the amide nitrogen [51]. In addition, it is notably to study the presence of an extra peak at 401.9 eV, which is contributed to nitrogen atom in protonated NH_x^+ groups. A similar N 1s peak was found at 402 ± 0.2 eV in previously reported values [50]. Therefore, these XPS results clearly indicate that the POAMA was covalently grafted onto the MWCNT surface successfully.

The contents of MWCNTs-COOH and MWCNTs-POAMA were also confirmed by TGA as compared in Fig. 4. For pristine MWCNTs, there is almost no weight loss below 500 °C, however, the onset of weight loss significantly occurs at a higher temperature than 500 °C, due to the thermal decomposition of the disordered carbon [52]. The organic part of functionalized MWCNTs could be degraded in the temperature range from 150 to 500 °C [53–56]. The weight loss of approximately 1.65% is detected for MWCNTs-COOH in the stage from 150 to 350 °C which is attributed to the decarboxylation of carboxylic groups present on the MWCNT walls [53]. Thermal degradation in the range between 350 and 500 °C can be explained by the elimination of hydroxyl functionalities which was grafted to the MWCNT walls [53]. Similarly, the major weight loss of MWCNTs-POAMA below 500 °C may be attributed to the decomposition of surface-grafted POAMA. Furthermore, the quantity of surface-grafted POAMA in MWCNTs can be calculated by comparing with the weight loss of pristine MWCNTs (Fig. 4) at 500 °C. Results indicate that the relative organic weight fraction of MWCNTs-POAMA is estimated as 10.29%. The values of mol% of the COOH groups and POAMA moieties with respect to carbon atoms in MWCNTs ($[COOH]_{MWCNTs}$ = 0.44 mol% and $[POAMA]_{MWCNTs}$ = 0.057 mol%, respectively) were calculated by using weight percent and molecular weight of the COOH groups and POAMA fragment, respectively [57]. The estimated mol% values implied that only ~13% carboxylic acid is converted to an amide leakage attached to the MWCNT walls due to the steric hindrance effect on the POAMA molecules. These results are in agreement with the TEM, XPS and TGA results and confirm that POAMAs have grafted onto the surface of MWCNTs effectively.

It is of interest to investigate the degree of dispersion of MWCNT within MWCNTs/VE nanocomposites as examined by SEM. The MWCNTs/VE nanocomposites are prepared by drop casting the styrene monomer solution mixture onto the clean aluminum substrates at 140 °C in an oven. The MWCNT content in the MWCNTs/VE nanocomposites was kept at 1 wt% in each sample. The cross sections of the nanocomposites were prepared by bending the samples to provide an intact fractured surface, and the SEM images are illustrated in Fig. 5. The SEM images of three MWCNTs/VE nanocomposites show different features. The SEM image of the fractured surface of the pristine MWCNTs/VE nanocomposite shows non-uniform dispersion (Fig. 5a). In addition, MWCNTs were pulled out from the matrix due to the poor adhesion between MWCNTs and the matrix, indicating a limited reinforcement. The nanocomposite reinforced by MWCNTs-COOH (Fig. 5b) exhibits a noticeably morphology of broken segments of MWCNT ropes rather than just pulled out, suggesting that the polar interaction existed among hydroxyl and carbonyl groups in VE polymers, and the carboxylic groups of MWCNTs-COOH help to disperse MWCNT bundles, resulting from the stronger MWCNTs–VE interaction [58,59]. By comparison, the MWCNTs-POAMA/VE nanocomposites possess better homogeneity and good dispersion on the fractured surface as shown in Fig. 5c (30,000×). The MWCNTs where embedded in the VE matrix. At high magnification (Fig. 5d, 100,000×) demonstrated that MWCNTs were completely coated by VE and that the diameter of coated MWCNTs (80 nm) was much larger than that of the pristine MWCNTs (30 nm). This suggests that MWCNTs were held tightly to the matrix, demonstrating a strong interaction between the VE matrix and the MWCNTs-POAMA. From the above observations, it implied that the terminal unsaturated double bonds of the POAMA were attached to the MWCNTs, an additional chemical bonding with the vinyl ester was existed, consequently, MWCNTs would be more compatible with the polymer matrix [33,28,59].

3.2. Mechanical properties of MWCNTs/VE nanocomposite bipolar plates

High-performance bipolar plates should provide the required mechanical strength for PEMFC applications. However, polymer composite bipolar plates with high graphite powder loading cannot easily be formed due to the weaker adhesion between the graphite and polymer matrix. The flexural strengths of MWCNTs/VE nanocomposite bipolar plates were measured as shown in Fig. 6. When the MWCNT content reached 2 wt%, the flexural strengths of VE nanocomposite bipolar plates consisting of pristine MWCNTs, MWCNTs-COOH and MWCNTs-POAMA are 37.51, 37.96 and 41.44 MPa, respectively (Fig. 6). Since CNTs have distinctly superior mechanical strength, they can improve the stiffness of composite bipolar plates effectively by adding a small quantity of MWCNTs. Accordingly, all of the MWCNTs/VE nanocomposite bipolar plates are stiffer than pure composite bipolar plates, which has a flexural strength of 28.54 MPa. It is believed that the increase in flexural strength is associated mainly with the rigidity, high-aspect ratio and functionalization of MWCNTs, which are critical in determining the mechanical properties of the resulting composite. The flexural strength of the nanocomposite bipolar plate with just 2 wt% loading of MWCNTs-POAMA shows more than 40% improve-

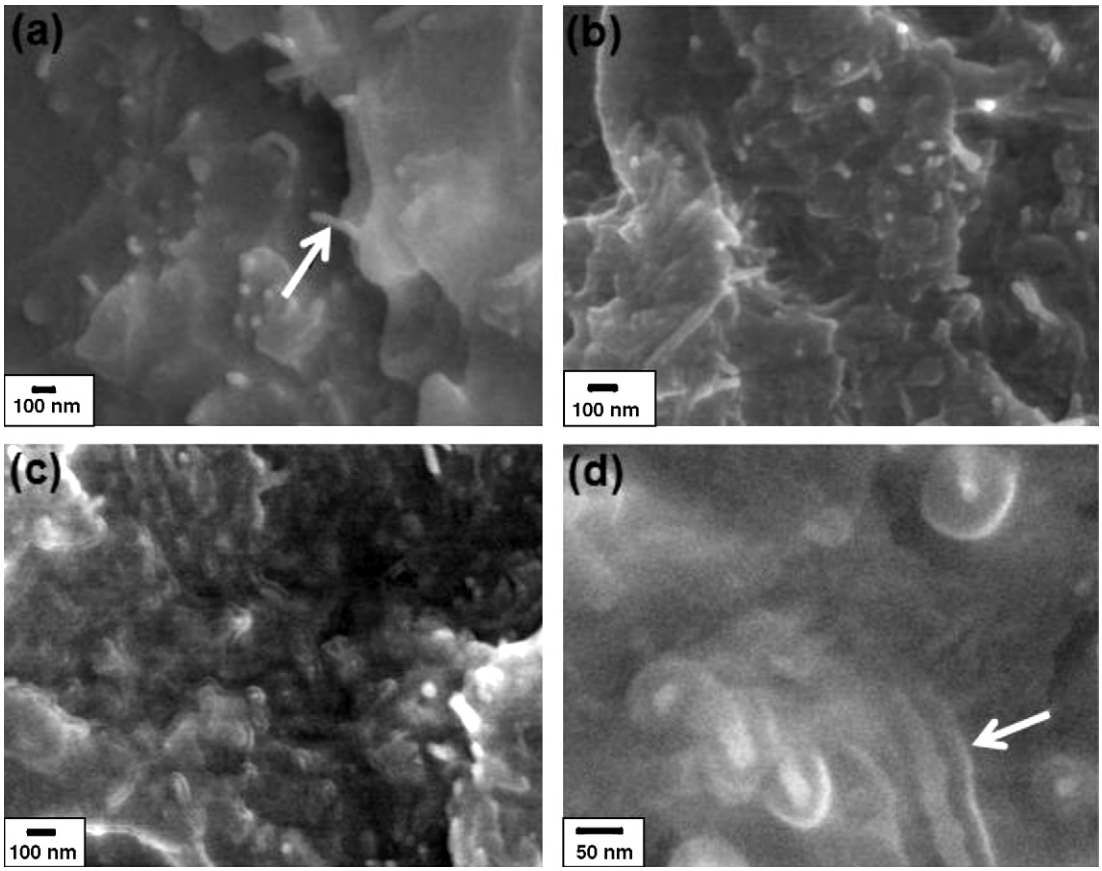

Fig. 5. SEM images of fractured surface of MWCNTs/VE nanocomposites with various MWCNTs including: (a) pristine MWCNTs (30,000×), (b) MWCNTs-COOH (30,000×), and (c and d) MWCNTs-POAMA (30,000× and 100,000×).

ment as compared to that of the pure composite bipolar plate, which may result from the stronger MWCNT–polymer interaction. From the SEM observation (Fig. 5c and d), this provides further evidence that the homogeneous dispersion of MWCNTs-POAMA promotes the formation of a filler–polymer network structure, causing the composite bipolar plate more efficiently to transfer the load from the host polymer matrix to MWCNTs [38,60]. Nevertheless, it is anticipated that the increase in the flexural strength is associated with the reinforcing role of MWCNTs that cause an improved MWCNT–vinyl ester interface due to the cross-linked POAMA attached on the MWCNTs with vinyl ester through a free-radical reaction.

Inorganic/organic composites often become stiff and more brittle upon incorporation of inorganic fillers. However, carbon nanotubes present a particular form of reinforcing fiber, with highly flexible elastic behavior due to a high-aspect ratio during loading, which are different from micrometer-sized fibers. Fig. 7 shows the unnotched impact strength of MWCNTs/VE nanocomposite bipolar plates as a function of MWCNT content. The unnotched impact strength is improved considerably by the inclusion of MWCNTs-

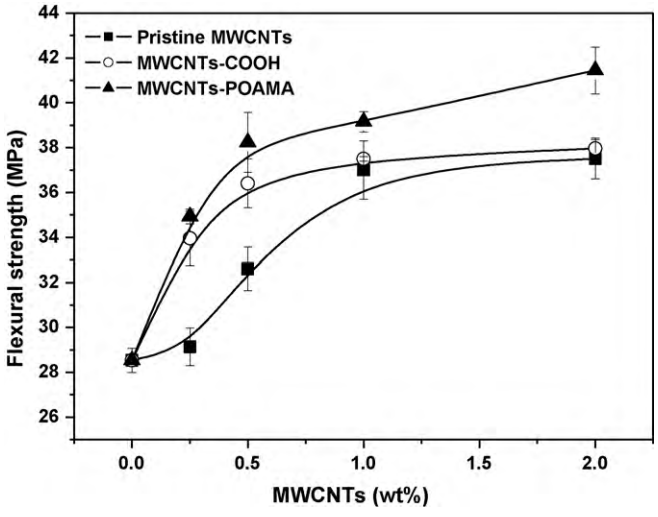

Fig. 6. The flexural strength of nanocomposite bipolar plates with various MWCNTs.

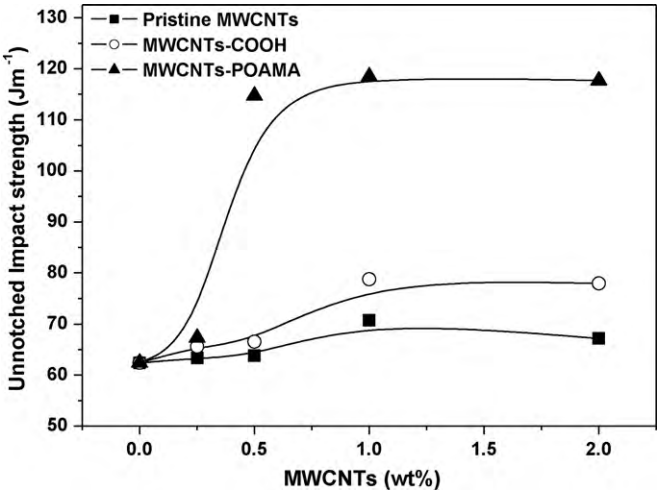

Fig. 7. The unnotched impact strength of nanocomposite bipolar plates with various MWCNTs.

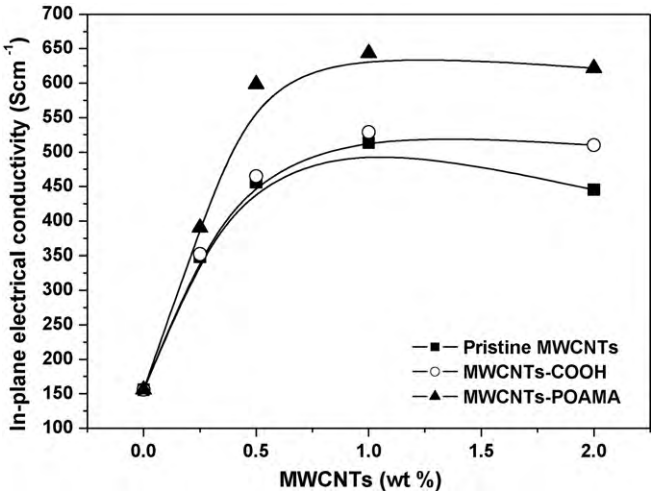

Fig. 8. In-plane electrical conductivity of nanocomposite bipolar plates with various MWCNTs.

POAMA in the VE nanocomposite bipolar plates as with the MWCNT content increased to 1 wt%, and then leveled off as MWCNTs loading increased up to 2 wt%. The MWCNTs-POAMA rather than MWCNTs-COOH exhibited much more increase of ultimate impact strength up to 118.5 J m^{-1}, which is a 90% increment as compared to pure composite bipolar plates. The improvement in unnotched impact strength of the compatible MWCNTs-POAMA/VE nanocomposite bipolar plates is due to the fact that the stronger the interfacial adhesions, the higher the impact strength. By means of strong interfacial bonding at the molecular level with cross-linked polymer chains, such behavior will contribute to continuous absorption of energy. Meanwhile, the stress transfer may arise easily from the uniform dispersion of MWCNTs. With strong covalent bonding, the MWCNTs-POAMA can offer extra benefits to increase the strain to failure, and thus will increase the fracture toughness and impact resistance for VE nanocomposite bipolar plates [33].

The improvement of flexural strength and unnotched impact strength reflects the immediate effective load transfer of carbon nanotubes through strong interfacial bonding due to a number of free terminal unsaturated double bonds of the POAMA attached on the carbon nanotubes. Cross-linking network was obtained by direct chemical bonding of these unsaturated double bonds to the vinyl ester matrix. These results support the theoretical and molecular simulation predictions of stress transfer, and hence, mechanical strength of carbon nanotubes–vinyl ester nanocomposite bipolar plates can be effectively increased by the addition of chemical bonding [59,61]. Nevertheless, pristine MWCNTs for reinforcement of nanocomposites have a very limited effect because of lack of interfacial bonding across the automatically smooth CNT surfaces, and therefore, exhibit very poor load-transfer ability [33,61].

3.3. In-plane electrical conductivity of MWCNTs/VE nanocomposite bipolar plates

A high in-plane (bulk) electrical conductivity is an essential feature for PEMFC bipolar plates. A percolating conducting path is necessary to achieve high electrical conductivity [62]. However, a thin layer of insulating polymer matrix with high electrical resistance along the conducting path increases the total path resistance. Therefore, graphites only contribute to limited conductivity of the composite bipolar plate. Fig. 8 exhibits the in-plane electrical conductivity of nanocomposite bipolar plates as a function of MWCNT content. It shows that in-plane electrical conductivity increases with MWCNT content for three systems. In-plane electrical conductivity increases significantly in the order of MWCNTs-POAMA > MWCNTs-COOH > pristine MWCNT nanocomposite bipolar plates, for a given MWCNT content. For the sample with 1 wt% of MWCNT content, the in-plane electrical conductivities of MWCNTs-POAMA, MWCNTs-COOH, and pristine MWCNT nanocomposite bipolar plates are measured at 643, 529 and 513 S cm^{-1}, respectively. For pristine MWCNTs, the formation of local MWCNT aggregations tend to increase the number of filler–filler hops required to traverse a given distance, thus causing the decrease of in-plane electrical conductivity at high MWCNT loading (2 wt%). Accordingly, the driving force for higher in-plane electrical conductivity of MWCNTs-POAMA/VE nanocomposite bipolar plates shows better dispersion of MWCNTs in the VE matrix, due to the adding of chemical cross-linking. The reason may be further explained as follows: the good dispersion of MWCNTs-POAMA in the VE matrix causes CNTs contact each other easily and thus constructs much more efficient electrical networks in the nanocomposite bipolar plate.

3.4. Contact resistance of MWCNTs/VE nanocomposite bipolar plates

Although the in-plane electrical conductivity of bipolar plates is an important factor, the performance of the bipolar plate in a fuel cell is a critical character. To evaluate the electrical properties of the bipolar plates in a fuel cell, contact resistance tests were conducted. A major source of contact resistance at an interface is a function of the properties of the gas diffusion layer and the bipolar plate. The contact resistance is commonly governed by the surface topography of the contacting pair. The current only flows through the contact asperities, leading to a reduction of voltage across the interface [63]. It is clear that when the contact pressure is applied at one component toward another one, the contact resistance decreases as pressure increases. The effect takes place because of the increase in contact area between fuel cell components under the load. Fig. 9 presented the comparisons of the contact resistance for various composite bipolar plates with compaction process. Furthermore, Fig. 9 shows the contact resistance of pristine MWCNTs, MWCNTs-COOH and MWCNTs-POAMA/VE nanocomposite bipolar plates with 1 wt% MWCNT content decrease with increasing pressure due to the fact that the actual area of contact between the asperity structures at the interface increases. However, with the increase of compaction pressure, the difference among various composite bipolar plates becomes smaller. And they were almost the same

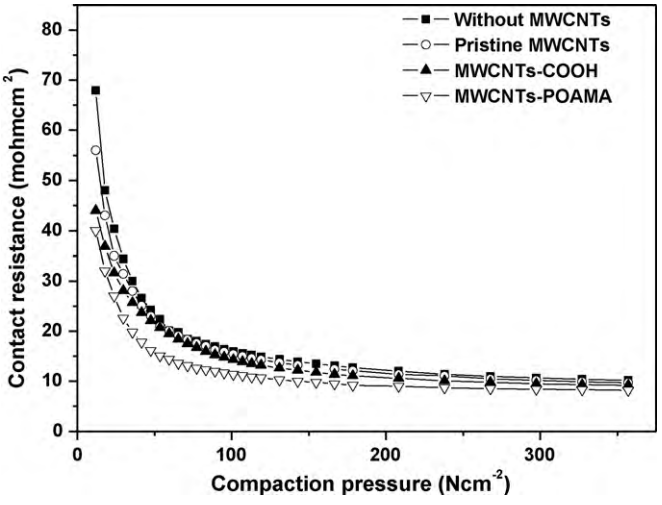

Fig. 9. Contact resistance of nanocomposite bipolar plates with various MWCNTs.

after 300 N cm^{-2}. At a compaction pressure of 140 N cm^{-2} (test condition specified by DOE) [64], contact resistance decreased in the order of MWCNTs-POAMA < MWCNTs-COOH < pristine MWCNTs < original composite bipolar plate and were measured to be 10, 12.2, 13.2 and 13.9 mohm cm^2, respectively. The dramatic decrease in contact resistance of the MWCNTs-POAMA/VE nanocomposite bipolar plates could be attributed to the fact that the excellent dispersion of MWCNTs would cause electron transfer uniformly in the MWCNTs-POAMA/VE nanocomposite bipolar plates.

In summary, the modification of MWCNTs grafted with POAMA, especially MWCNTs-POAMA, is a useful reinforcing method for producing suitable composite bipolar plates. The MWCNTs-POAMA reinforced vinyl ester/nanocomposite bipolar plates offer considerable scope for improving the mechanical strengths and electrical properties of the bipolar plates by improving the dispersion of carbon nanotubes or by modulating the interface with the polymer matrix [61].

3.5. Single fuel cell performance of MWCNTs/VE nanocomposite bipolar plates

Fig. 10 presents the performance of the single cells compressively assembled with pristine MWCNTs, MWCNTs-COOH, MWCNTs-POAMA nanocomposite bipolar plates, and pure composite bipolar plates without MWCNTs, respectively. The open circuit voltage (OCV) of single cells is almost the same at 1.0 V. Furthermore, the single cell incorporated with various 1 wt% MWCNT nanocomposite bipolar plates performs comparably with pure composite bipolar plates. All MWCNT nanocomposite bipolar plates obviously outperform the original composite bipolar plates without MWCNTs. Results reflect that the performance of the PEMFC was improved significantly by introducing MWCNTs. This improvement could be attributed to the fact that by compression molding the MWCNT nanocomposite bipolar plates, MWCNTs form an additional compact electrical network owing to MWCNT–MWCNT contacts. The current density of single cells increases in the order of using MWCNTs-POAMA > MWCNTs-COOH > pristine MWCNTs > pure composite bipolar plates without MWCNTs; the maximum current densities are 1.23, 1.11, 1.08, and 1.04 A cm^{-2}, respectively. Moreover, the maximum power density of the single cell consisting of MWCNTs-POAMA nanocomposite bipolar plates is 0.518 W cm^{-2}, 32% higher than that of pure composite bipolar plates without MWCNTs (0.392 W cm^{-2}). The nanocomposite bipolar plates-MWCNTs-POAMA presented in this study provide promising results for two reasons: (1) the dispersion of MWCNTs-POAMA is better than the dispersion associated with other MWCNTs and (2) more continuous electrical conducting paths which promote the transfer of electrons in PEMFC.

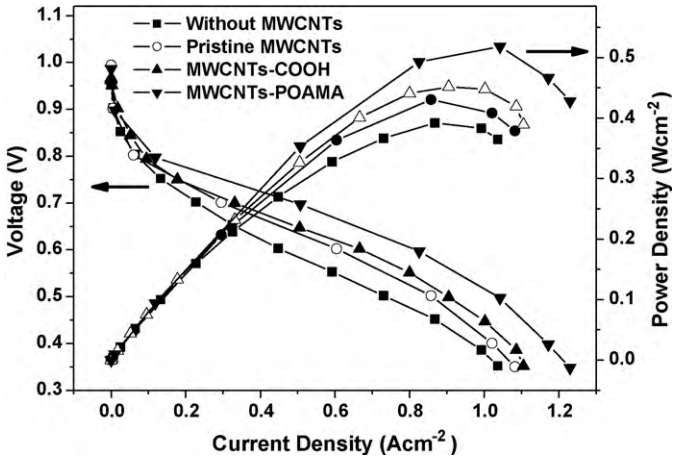

Fig. 10. Performance of the single cells assembled with pristine MWCNTs, MWCNTs-COOH, MWCNTs-POAMA, and without MWCNT composite bipolar plates.

4. Conclusions

A unique system of carbon nanotubes–vinyl ester cross-linking structure for composite bipolar plates in PEMFCs was developed in this work. The terminal unsaturated double bonds of the POAMA attached to the MWCNTs can readily react with the vinyl ester and act as cross-links for vinyl ester matrix, while bifunctional vinyl ester continues to react with the styrene monomer curing agents added. The SEM images of MWCNTs/VE nanocomposites show that the MWCNTs/POAMA possess higher dispersity of MWCNTs inside the VE matrix. This may be due to the terminal unsaturated double bonds of the POAMA causes MWCNTs-POAMA generate an effectively chemical bonding between the VE matrix and the carbon nanotubes. Moreover, the mechanical, electrical property and contact resistance of the MWCNTs/POAMA nanocomposite bipolar plate were increased significantly, due to the better dispersion of MWCNTs, consequently, higher mechanical strength, superior electrical conductivity and lower interfacial contact resistance can be achieved. The MWCNTs-POAMA/VE nanocomposite bipolar plates also exhibit significant enhancement in fuel cell performance compared to the pure composite bipolar plate, especially, at higher current and power densities, due to more continuous conducting paths resulting in better electron transfer in PEMFC. The overall performance shows that the VE nanocomposite bipolar plates with MWCNTs-POAMA developed in this work perform excellently for PEMFCs.

Acknowledgements

The authors were grateful to Fuel Cell Center of Yuan Ze University, Taiwan, for assistance with the instrumentations and the National Science Council, Taiwan, Republic of China under contract NSC-98-ET-E-007-009-ET for the financial support.

References

[1] S.H. Liao, C.H. Hung, C.C.M. Ma, C.Y. Yen, Y.F. Lin, C.C. Weng, J. Power Sources 176 (2008) 175.
[2] B.D. Cunningham, J. Huang, D.G. Baird, J. Power Sources 165 (2007) 764.
[3] S.H. Liao, C.Y. Yen, C.C. Weng, Y.F. Lin, C.C.M. Ma, C.H. Yang, M.C. Tsai, M.Y. Yen, M.C. Hsiao, S.J. Lee, X.F. Xie, Y.H. Hsiao, J. Power Sources 185 (2008) 1225.
[4] G.O. Mepsed, J.M. Moore, Handbook of Fuel Cells—Fundamentals, Technology and Application, John Wiley and Sons, Ltd., New York, 2003, pp. 286–293.
[5] A.A. Kulikovsky, J. Power Sources 160 (2006) 431.
[6] T. Yang, P. Shi, J. Power Sources 175 (2008) 390.
[7] M.S. Wilson, D.W. Busick, US Patent 6,248,467 (2001).
[8] B.D. Cunningam, D.G. Baird, J. Mater. Chem. 16 (2006) 4385.
[9] J. Wind, A. La Croix, S. Braeuninger, P. Hedrich, C. Heller, M. Schudy, Handbook of Fuel Cells—Fundamentals, Technology and Application, John Wiley and Sons, Ltd., New York, 2003, pp. 295–307.
[10] C.Y. Bai, Y.H. Chou, C.L. Chao, S.J. Lee, M.D. Ger, J. Power Sources 183 (2008) 174.
[11] H. Tawfik, Y. Hung, D. Mahajan, J. Power Sources 163 (2007) 755.
[12] S.-T.K. Hong, K.S. Weil, J. Power Sources 168 (2007) 408.
[13] K. RoBberg, V. Trapp, Handbook of Fuel Cells—Fundamentals, Technology and Application, John Wiley and Sons, Ltd., New York, 2003, pp. 308–314.
[14] J.K. Kuo, C.K. Chen, J. Power Sources 162 (2006) 207.
[15] I.E. Paulauskas, M.P. Brady, H.M. Meyer III, R.A. Buchanan, L.R. Walker, Corros. Sci 48 (2006) 3157.
[16] H.C. Kuan, C.C.M. Ma, K.H. Chen, S.M. Chen, J. Power Sources 134 (2004) 7.
[17] S.H. Liao, C.Y. Yen, C.H. Hung, C.C. Weng, M.C. Tsai, Y.F. Lin, C.C.M. Ma, C. Pan, A. Su, J. Mater. Chem. 18 (2008) 3993.
[18] M. Wu, S.L. Leon, J. Power Sources 136 (2004) 37.
[19] L.D. Andrew, J. Power Sources 156 (2006) 128.
[20] R.C. Emanuelson, W.L. Luoma, W.A. Taylor, US Patent 4,301,222 (1981).
[21] B.B. Fitts, V.R. Landi, S.K. Roy, US Patent 6,911,917 (2004).
[22] G.W. Yeager, M. Cavazos, H. Guo, G.D. Merfeld, J. Rude, E.O. Teutsch, K.P. Zarnoch, US Patent 6,905,637 (2005).
[23] C.C.M. Ma, K.H. Chen, H.C. Kuan, S.M. Chen, M.H. Tasi, Y.Y. Yen, F.H. Tsau, US Patent 7,090,793 (2006).
[24] S. Li, Y.J. Qin, Z. Shi, X. Guo, Y. Li, D. Zhu, Chem. Mater. 17 (2005) 130.

[25] R.H. Banughman, A.A. Zakhidov, W.A. der Heer, Science 297 (2002) 787.
[26] R. Haggenmueller, J. Chen, H.Y. Liu, Appl. Phys. Lett. 83 (2003) 2928.
[27] C.H. Tseng, C.C. Wang, C.Y. Chen, Chem. Mater. 19 (2007) 308.
[28] L. Sun, G.L. Warren, J.Y. O'Reilly, W.N. Everett, S.M. Lee, D. Davis, D. Lagoudas, H.-J. Sue, Carbon 46 (2008) 320.
[29] S. Wang, R. Liang, B. Wang, C. Zhang, Chem. Phys. Lett. 457 (2008) 371.
[30] G.L. Hwang, Y.T. Shieh, K.C. Hwang, Adv. Funct. Mater. 14 (2004) 487.
[31] R. Blake, J.N. Coleman, M.T. Byrne, J.E. McCarthy, T.S. Perova, W.J. Blau, A. Fonseca, J.B. Nagy, Y.K. Gun'ko, J. Mater. Chem. 16 (2006) 4206.
[32] H. Xia, M. Song, J. Mater. Chem. 16 (2006) 1843.
[33] J. Zhu, H. Peng, F. Rodriguez, J.L. Margrave, V.N. Khabashesku, A.M. Imam, K. Lozano, E.V. Barrera, Adv. Funct. Mater. 14 (2004) 643.
[34] O. Lourie, H.D. Wagner, Appl. Phys. Lett. 73 (1998) 3527.
[35] P. Calvert, Nature 399 (1999) 210.
[36] A. Star, J.F. Stoddart, D. Steuerman, M. Diehl, A. Boukai, E.W. Wong, X. Yang, S.W. Chung, H. Choi, J.R. Health, Angew. Chem. Int. Ed. 40 (2001) 1721.
[37] J.L. Bahr, J.M. Tour, J. Mater. Chem. 12 (2002) 1952.
[38] Z.H. Fan, K.T. Hsiao, S.G. Advani, Carbon 42 (2004) 871.
[39] O. Gryshchunk, J. Karger-Kocsis, R. Thomann, Z. Konya, I. Kirics, Compos. A 37 (2006) 1252.
[40] E.T. Thostenson, S. Ziaee, T.W. Chou, Compos. Sci. Technol. 69 (2009) 801.
[41] S. Wang, Z. Liang, T. Liu, B. Wang, C. Zhang, Nanotechnology 17 (2006) 1551.
[42] N. Grossiord, J. Loos, O. Regev, C.E. Kaning, Chem. Mater. 18 (2006) 1089.
[43] J. Zhu, J. Kim, H. Peng, J.L. Margrave, V.N. Khabashesku, E.V. Barrera, Nano Lett. 3 (2003) 1107.
[44] S. Wang, Z. Liang, P. Gonnet, Y.H. Liao, B. Wang, C. Zhang, Adv. Funct. Mater. 17 (2007) 87.
[45] M.S. Arnold, M.O. Guler, M.C. Hersam, S.I. Stupp, Langmuir 21 (2005) 4705.
[46] T.I.T. Okpalugo, P. Papakonstantinou, H. Murphy, J. McLaughlin, N.M.D. Brown, Carbon 43 (2005) 153.
[47] H. Ago, T. Kugler, F. Cacialli, W.R. Salaneck, M.S.P. Shaffer, A.H. Windle, R.H. Friend, J. Phys. Chem. B 103 (1999) 8116.
[48] J.F. Moulder, W.F. Stickle, P.E. Sobol, K.D. Bomben, Handbook of X-ray Photoelectron Spectroscopy, Perkin-Elmer Corporation, Eden Prairie, MN, 1992.
[49] S.A. Evenson, C.A. Fail, J.P.S. Badyal, Chem. Mater. 12 (2000) 3038.
[50] C.M. Pradier, C. Rubio, C. Poleunis, P. Bertrand, P. Marcus, C. Compre, J. Phys. Chem. B 109 (2005) 9540.
[51] Y. Liu, S.H. Goh, S.Y. Lee, Macromolecules 32 (1999) 1947.
[52] Y.L. Hsin, K.C. Hwang, C.T. Yeh, J. Am. Chem. Soc. 129 (2007) 9999.
[53] V. Datsyuk, M. Kalyva, K. Papagelis, J. Parthenios, D. Tasis, A. Siokou, I. Kallitsis, C. Galiotis, Carbon 46 (2008) 833.
[54] A.D. Christopher, M.T. James, Nano Lett. 3 (2003) 1215.
[55] H.M. Huang, C.Y. Chang, H.C. Tsai, C.H. Hsu, R.C. Tsiang, I.C. Liu, Macromolecules 37 (2004) 283.
[56] S. Chen, W. Shen, G. Wu, D. Chen, M. Jiang, Chem. Phys. Lett. 402 (2005) 312.
[57] Calculated according to the following equation: i.e. $[COOH]_{MWCNTs} = [(\text{weight \% of COOH from TGA/mol wt of COOH groups})/(100/\text{mol wt of carbon})] \times 100$. D. Baskaran, J.W. Mays, M.S. Bratcher, Angew. Chem. Int. Ed. 43 (2004) 2138.
[58] R. Sen, B. Zhao, D. Perea, M.E. Itkis, H. Hu, J. Love, E. Bekyarova, R.C. Haddon, Nano Lett. 4 (2004) 459.
[59] J. Gao, B. Zhao, M.E. Itkis, E. Bekyarova, H. Hu, V. Kranak, A. Yu, R.C. Haddon, J. Am. Chem. Soc. 128 (2006) 7492.
[60] H. Geng, R. Rosen, B. Zheng, H. Shimoda, L. Fleming, J. Liu, et al., Adv. Mater. 14 (2002) 1387.
[61] S.J.V. Frankland, A. Caglar, D.W. Brenner, M. Griebel, J. Phys. Chem. B 106 (2002) 3046.
[62] H. Wolf, M. Willert-Porada, J. Power Sources 153 (2006) 41.
[63] A. Kraytsberg, M. Auinat, Y. Ein-Eli, J. Power Sources 164 (2007) 697.
[64] US car & Fuel Cell Partnership. Fuel Cell Technologies Roadmap, available at http://www.uscar.org/commands/files_download.php?files_id=81, August 2005.